HHS Public Access

Author manuscript

Mater Today (Kidlington). Author manuscript; available in PMC 2020 December 01.

Published in final edited form as:

Mater Today (Kidlington). 2019 December ; 31: 86–99. doi:10.1016/j.mattod.2019.06.003.

Magnetic Iron Oxide Nanoparticles for Disease Detection and Therapy

Sheng Tong, **Haibao Zhu**, **Gang Bao***

Department of Bioengineering, Rice University, Houston, Texas 77030, USA

Abstract

Magnetic iron oxide nanoparticles (MIONs) are among the first generation of nanomaterials that have advanced to clinic use. A broad range of biomedical techniques has been developed by combining the versatile nanomagnetism of MIONs with various forms of applied magnetic fields. MIONs can generate imaging contrast and provide mechanical/thermal energy *in vivo* in response to an external magnetic field, a special feature that distinguishes MIONs from other nanomaterials. These properties offer unique opportunities for nanomaterials engineering in biomedical research and clinical interventions. The past few decades have witnessed the evolution of the applications of MIONs from conventional drug delivery and hyperthermia to the regulation of molecular and cellular processes in the body. Here we review the most recent development in this field, including clinical studies of MIONs and the emerging techniques that may contribute to future innovation in medicine.

Graphical Abstract

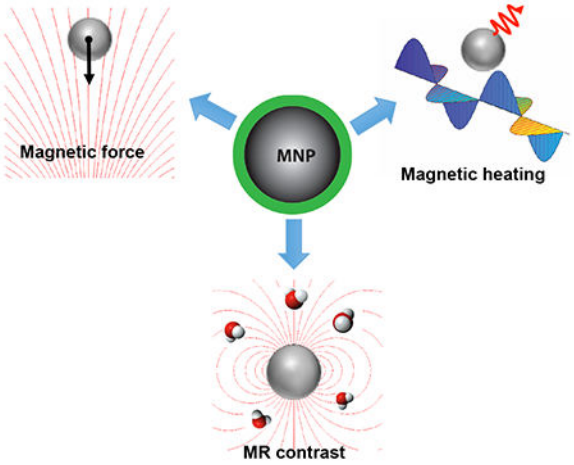

*Correspondence should be addressed to Gang Bao (gang.bao@rice.edu).

Introduction

Magnetic iron oxide nanoparticles (MIONs) typically refer to the materials that consist of magnetite (Fe_3O_4) or maghemite (γ-Fe_2O_3) and have a size ranging from 1 to 100 nm. MIONs can disperse in biological fluids as a result of Neelian and Brownian relaxations and yet respond to an external magnetic field. This intriguing feature has attracted tremendous interests in biomedical research since the 1970s. The earliest studies of MIONs were naturally directed toward magnetic targeting, i.e., using a magnetic field to remotely control the distribution of drug molecules in the body, thereby enhancing drug accumulation in the target tissue [1–4]. After nearly 40 years, magnetic targeting remains to be an active research area and the cargos of MIONs have expanded from small molecule drugs to a vast array of therapeutic agents including proteins, nucleotides, viral vectors, immune cells, and stem cells [5–9]. In the meantime, MIONs have manifested many other important properties, which offer great promises for biomedical applications ranging from interrogating molecular and cellular events in basic research to disease detection, diagnosis, and treatment.

The magnetic properties of magnetite and maghemite nanocrystals are distinct from those of bulk materials owing to the unique quantum mechanical effects at the nanoscale. At the length scale less than the magnetic domain wall width (ca. 80-90 nm), these nanocrystals support only one magnetic domain, in which the spins of unpaired electrons are coupled to behave as a macro magnetic spin [10]. As the nanocrystal size further decreases below a superparamagnetic limit (ca. 20 nm), the thermal fluctuation becomes large enough to overcome the energy barrier arising from the magnetic anisotropy [10]. The magnetic anisotropy of nanocrystals, which involves the contribution from crystalline, shape and surface anisotropy, form a convoluted energy profile with several easy axes (the directions with minimum energy) [11]. The magnetic moment of individual nanocrystals flips rapidly among the easy axes, a process known as Neelian relaxation, and no net magnetization can be observed (Figure 1A). The magnetization of the nanocrystals will rapidly approach saturation magnetization when exposed to a modest magnetic field (0.2~0.5 T). These nanocrystals are thus named superparamagnetic iron oxide nanoparticles (SPIO) in comparison to paramagnetic ions such as Gd^{3+}. The nanocrystals with sizes beyond the superparamagnetic limit, e.g., ferromagnetic nanocrystals, show size-dependent remanence and coercivity [12]. It should be noted that the Brownian motion contributes to the magnetic relaxation of the nanocrystals dispersed in the solution. Another important feature of the nanocrystals is the large surface area to volume ratio. Due to the influence of the surface layer, the saturation magnetization and the magnetic anisotropy of the nanocrystals deviate significantly from those of bulk materials [13,14]. Importantly, these magnetic properties can be tuned by changing the size and shape of the nanocrystals, introducing core-shell coupling, doping iron oxide with other metal elements, or forming nanoclusters by crosslinking or encapsulation [12,15–22]. For simplicity, we will use the term MION to refer to all types of magnetic iron oxide nanomaterials.

The microscopic properties of MIONs give rise to a diverse range of functions in various static or dynamic magnetic fields, which provide unparalleled possibilities for probing and controlling a biological system. The biomedical applications of MIONs can be broadly divided into three categories according to the underlying mechanisms (Table 1 **and** Figures

1B, C, **and** D). First, as nanoscale magnets, MIONs experience a force in a nonuniform magnetic field and tend to move against the field gradient [23]. The magnetic mobility of MIONs is the physical basis for the magnetic separation of biomolecules and cells, *in vitro* magnetofection, and *in vivo* magnetic drug targeting [4–8,24,25]. More recently, MIONs have shown promises as a molecular force transducer for activating cell surface receptors, controlling the structure of the cytoskeleton, and triggering cell differentiation or apoptosis [26–30]. The second category is focused on the nonuniform local magnetic field generated by MIONs, which can be harnessed for T_1 or T_2 contrast in magnetic resonance imaging (MRI). MIONs have been utilized extensively as MRI contrast agents for cell tracking and molecular imaging since the 1980s [31–34]. The third category is associated with the capability of MIONs to convert electromagnetic energy into thermal energy, a phenomenon named as magnetic nanoparticle heating (MNH) [35]. There is a great interest in developing MNH for cancer hyperthermia and organ preservation [36,37]. Furthermore, increasing evidence has indicated that MIONs can be employed as a point heat source to induce the conformational change of heat-sensitive proteins, which enables remote control of cell signaling molecules or ion channels [35,38–40].

The magnetic functions of MIONs greatly enrich the arsenal for fighting critical diseases, especially cancer. In the last two decades, MION-enhanced MRI and magnetic hyperthermia have been translated from bench to bedside [37,41,42]. In preclinical studies, many other MION-based technologies have shown far-reaching implications for precision and personalized medicine. Herein, we will review the most recent findings in the synthesis and biomedical applications of MIONs, including up-to-date clinical studies of MIONs and the emerging applications of MIONs that may contribute to novel therapeutic schemes. In this review the applications of MIONs are discussed in three sections: magnetic targeting, diagnostic imaging, and magnetic nanoparticle hyperthermia, which summarize the applications related to the mechanical, imaging, and thermal effects of MIONs respectively.

Magnetic nanoparticle synthesis

MIONs used in biomedical applications consist of iron oxide nanocrystals and the molecules that coat the crystal surface, provide the link to functional groups, and interface with the biological system. The functions of MIONs *in vivo* may depend on not only the magnetic properties but also its toxicity, immunogenicity, biodistribution, and metabolism. Magnetite and maghemite nanocrystals are the most commonly used magnetic nanomaterials, thanks to their good magnetization and minimal toxicity. Many important magnetic properties of magnetite and maghemite nanocrystals are size-dependent [12–14,43]. Therefore, generating uniform nanocrystals at the desired sizes is critical to most applications. The immunogenicity and the biodistribution of MIONs are determined by a number of biophysical factors that are associated with both the nanocrystal itself and the coating molecules, which can be tailored through nanocrystal synthesis and post-synthesis surface modification [44]. Further, clinical applications of MIONs often demand large-scale and consistent production of nanocrystals, as well as high-quality coating and functionalization. A plethora of synthesis methods ranging from conventional solution-based synthesis, to vapor deposition and lithography have been developed to address these challenges [45].

The two most widely used synthesis methods are coprecipitation and thermodecomposition. In the coprecipitation method, ferrous and ferric salts, e.g., $FeCl_2$ and $FeCl_3$, are mixed stoichiometrically in an aqueous medium. Iron oxide nanocrystals are generated by precipitating the ferrous and ferric ions with a base, e.g., NaOH. Coprecipitation is often performed in the presence of hydrophilic polymers such as dextran or starch, which bind to the iron oxide and form a hydrophilic and biocompatible surface. The resulting nanoparticles can disperse well in most biological fluids. The coprecipitation method is simple, cost-effective, and suitable for large-scale synthesis. Thus, to date, most MIONs for biomedical applications are produced via coprecipitation [42,46]. However, it offers little control over crystal growth. The nanocrystals are small (< 10 nm), poorly crystalline and polydispersed [47]. Post-synthesis size selection, e.g., size-exclusion chromatography, is often used to obtain MIONs at the desired size [31]. However, selected nanoparticles may contain one or multiple nanocrystals and variable amount of coating polymer, which makes stoichiometric functionalization challenging.

Over the past two decades, the need to control the size distribution of nanocrystals has led to the development of the thermodecomposition method. Here the precursor compounds such as iron pentacarbonyl, iron oleate or iron acetylacetonate, are decomposed in organic solvents at high temperature, generating the “Fe-O” species in a controllable manner [16,17,48]. The “Fe-O” monomers will either nucleate to form new nanocrystals or add onto the surface of existing nanocrystals depending on its concentration [49]. Importantly, the thermodecomposition method facilitates the separation of the nucleation and crystal growth processes, which is the prerequisite for producing monodispersed nanocrystals [16,49–51]. Many studies have shown that highly uniform magnetite and maghemite nanocrystals from ~4 nm to >100 nm can be synthesized by adjusting the reaction conditions such as the concentration of the precursor compound, the ratio between the precursor and the complexing agents, solvents, and incubation temperature, etc. (Figure 2A) [16–18,43,52]. The morphology of the nanocrystals can be altered to some extent by limiting the growth to specific facets of the nanocrystals [20,53]. The thermodecomposition method can also be scaled up, although to a less extent compared with the coprecipitation method. Park et al. has demonstrated the synthesis of 40 g iron oxide nanocrystals in one reaction, which is clinically relevant given that the recommended MRI dose for Feraheme®, a FDA-approved formulation of MION, is 1.02 g for a 70-kg adult [17,54].

In addition to size tuning, the magnetic properties of MIONs can be modified by changing the chemical composition of nanocrystals or generating clusters of magnetic nanocrystals. Several studies have shown that the salts of cobalt, manganese, and zinc can be mixed with iron precursors to generate doped metal ferrite nanocrystals [32,55]. Doped metal ions shift the balance between the ferrous and ferric ions occupying the tetrahedral and octahedral sites in the crystal, thereby increasing the net magnetization per unit cell [32]. For example, MIONs doped with Zn and Mn have a saturation magnetization of 175 emu/g (Zn+Mn+Fe), much higher than that of magnetite nanocrystals (114 emu/g(Fe)) [55]. Clusters of magnetite nanocrystals can be generated by adding polymers such as polyacrylic acid (PAA) in the synthesis [19]. PAA crosslinks nanocrystals through its many carboxylate groups that form coordination with iron cations on the surface of the nanocrystals (Figure 2B). In the nanoclusters, each nanocrystal is subjected to the magnetic field of its neighbors, which

alters its response to the external magnetic field. In contrast to single magnetite crystals of similar size, the nanoclusters can be a few hundred nanometers in diameter but remain superparamagnetic [19].

Other than chemical synthesis, many studies have shown that MIONs can be generated by organisms ranging from bacteria to mammals. Magnetotactic bacteria such as *M. magnetotacticum* can form a chain of magnetosomes in its body and use it to sense the magnetic field of the earth (Figure 2C) [56]. The bacterial magnetosomes showed high heating efficiency compared to many synthetic MIONs [57,58]. Interestingly, the mammalian cells transfected with magA or Mms6, genes used by *M. magneticum* to form magnetosomes, can also generate MIONs [59–61]. Another biosynthesis pathway is mediated by a highly conserved metalloprotein, ferritin. Mammalian cells, e.g., mesenchymal stem cells, can generate MIONs encapsulated in a ferritin nanocage as part of the iron metabolism in the body [62]. The ferritin-coated MIONs can be induced *in vivo* by transfecting the target cells with the ferritin gene [63,64]. The biosynthesis of MIONs may circumvent the issues associated with delivering exogenous MIONs into the body.

For biomedical applications, surface coating of MIONs forms the interface between the nanocrystals and the biological system that consists mostly of aqueous media. Some as-synthesized MIONs are coated with hydrophilic molecules. For example, during nanocrystal synthesis with coprecipitation, dextran or starch can be introduced as the capping molecules. These coating molecules can be further modified and conjugated with functional moieties, such as targeting ligands, drug molecules, and imaging contrast agents [65]. The nanocrystals synthesized by thermodecomposition are commonly coated with hydrophobic fatty acids, and dispersible only in nonpolar solvents. Water-dispersible MION can be generated by replacing the capping molecules with hydrophilic molecules through surface ligand exchange [66–68]. Alternatively, hydrophobic nanocrystals can be encapsulated by amphiphilic molecules to form a hydrophilic surface [69]. Poly(ethylene glycol) (PEG) is often the preferred coating molecule because of its stability, biocompatibility, low immunogenicity, and the ability to minimize protein binding. Other important coating materials include mesoporous silica, poly(lactic-co-glycolic acid), lipids, and proteins [70–72]. Similar to other nanomaterials, MIONs can be functionalized with various molecules including proteins, such as cytokines and antibodies, nucleic acids, such as aptamers, siRNA, mRNA or DNA plasmid, and small molecules, including fluorophores, radioisotopes, drug molecules, and other therapeutic agents (more details can be found in ref [73]).

In addition to providing water-dispersity and conjugation sites, the coating molecules play important roles in the biological functions of MIONs. The density, thickness and charge of the coating layer affect the colloidal stability of MIONs. In systemic circulation, a wide spectrum of plasma proteins including fibrinogen, albumins, and opsonins (immunoglobulins, complement factors, etc.) can be adsorbed onto the surface of nanoparticles, which is often described as the formation of a protein corona. The composition of the protein corona is determined by both the size and shape of the nanocrystal and the physiochemical properties of the coating layer [74]. The formation of the protein corona can increase the clearance of nanoparticles from the circulation and

change the interactions of nanoparticles with the target cells [75,76]. The coating molecules may also induce hypersensitivity/anaphylaxis reactions, such as those noted for Feraheme® in clinical applications. Therefore, coating optimization is indispensable to the biomedical applications of MIONs.

Magnetic targeting

Conventional drug delivery methods rely on intrinsic biotransport processes in the human body, such as the blood flow, the permeation in the tissue matrices, and cellular uptake. Over millions of years of evolution, these processes have been perfected for the efficient supply of oxygen and nutrients to all the cells in the body. However, they are unfavorable to the delivery of many therapeutic agents, in particular, agents for cancer chemotherapy. Many chemotherapeutic agents have a low therapeutic index, i.e., they are toxic to both cancerous and normal cells at a similar concentration. Typically distributed throughout the body, chemotherapeutic agents can cause a range of adverse effects that limit the therapeutic options for cancer patients. Thus, magnetic targeting of therapeutics has attracted extensive research activities with the goal that, by directing the carriers of drug molecules with a magnetic field, they can preferentially accumulate in the target tissue, which helps reduce the side effects.

In magnetic targeting, drug molecules are typically loaded onto MIONs via either physical adsorption or chemical conjugation. After MIONs are administrated into the systemic circulation, a magnetic field applied to the target tissue sequestrates MIONs flowing through nearby blood vessels and subsequently enhances their extravasation from the vessels and penetration into the tissue. The magnetic force exerted on MIONs is given by

$$\boldsymbol{F} = \mu(\boldsymbol{m} \cdot \nabla)\boldsymbol{H} \tag{1}$$

where μ is the magnetic permeability of the tissue, $\boldsymbol{m}$ is the magnetic moment of MIONs, which is proportional to the volume of MIONs, and $\boldsymbol{H}$ is the magnetic field strength [77]. In the bloodstream, the applied magnetic force needs to overcome the blood flow-induced drag force that is proportional to the radius of MIONs. For this reason, large MIONs such as microspheres or clusters of small nanocrystals are more efficient for magnetic targeting. According to Samuel Earnshaw's theorem, the magnetic force cannot create a stable trap in the interior of a subject [78]. It suggests that MIONs will always move toward the magnet or the body surface if the magnets are placed externally. Previous studies have shown that MIONs can be concentrated at the center of a medium by a dynamic field, but it is unknown whether these dynamic magnetic systems are feasible for magnetic targeting in a human body [79,80]. Nevertheless, the movement of MIONs in the body is confined by the blood vessels as well as the pores and the fibers in the tissue. The effectiveness of magnetic targeting is collectively determined by the magnetic properties of MIONs, the applied magnetic field, and the anatomic and microscopic features of the target tissue including the geometry and density of the vascular network, the blood flow, the porosity of the vessel wall, and the permeability of the tissue stroma.

Magnetic drug targeting was first demonstrated with the magnetic microspheres formed of albumin, magnetite nanocrystals and doxorubicin, a chemotherapeutic agent, in the rat tail [1]. Subsequently, the magnetic targeting of MIONs carrying chemotherapeutic drugs, such as doxorubicin, epirubicin, and mitoxantrone, were investigated in various mouse, rat, and rabbit tumor models [4,81,82]. In these studies, the drug carriers were the clusters (> 100 nm) of small magnetite nanocrystals [82]. After injection into the bloodstream, these clusters were prone to the clearance by the mononuclear phagocytic system (MPS), which could rapidly remove the clusters from the circulation, thereby reducing their availability to the tumor site. A study in the rabbit model showed that infusing the drug-loaded MIONs directly into the tumor-feeding artery achieved sufficient drug accumulation in the tumor and induced a complete tumor remission [4]. In contrast, intravenous injection of the MIONs reduced tumor expansion but failed to shrink the tumor, which highlighted the importance of improving the bioavailability of MIONs in magnetic targeting. Importantly, these studies prove that magnetic targeting could reduce the drug dosage required for cancer treatment as well as systemic toxicity to the animals compared to that of the free drug molecules [4].

Encouraged by these findings, several clinical studies have been conducted for cancer patients with locally advanced tumors (Table 2). Lubbe et al. performed the first phase I clinical trial using MIONs loaded with epirubicin in 14 patients that had metastatic breast cancer, chondrosarcoma, squamous cell carcinoma of the parotis and hypopharynx, Ewing sarcoma, and malignant histiocytoma, all of which could be easily accessed by permanent block magnets [83]. This study showed that magnetically targeted epirubicin was well tolerated by the patients. MIONs were successfully directed to the tumor in half of the patients as examined by MRI. However, the efficacy of magnetic targeting needed to be further increased for cancer treatment. Other clinical trials were performed for magnetic targeted carriers-doxorubicin (MTC-DOX) in patients with inoperable hepatocellular carcinoma (NCT00041808 phase I/II, NCT00054951 phase I/II). MTC-DOX, formed by 0.5~5 μm elementary iron particles with an activated carbon surface [84], was administrated into the tumor via hepatic arterial infusion, while an external magnet was placed onto the tumor (Figures 3) [84]. Localization of MTC-DOX to the tumor was successful in most of the patients, and patients treated with MTC-DOX had a low or undetectable level of doxorubicin in the plasma, with no clinically significant toxicity observed. However, a follow-up large-scale clinical trial (NCT00034333 phase II/III) stopped prematurely because the treatment provided no improvement in the median survival time. The reason for the poor therapeutic outcome is not known. Lessons from Doxil®, the first FDA-approved nano-drug, showed that the therapeutic efficacy of nanoformulations is often less prominent in cancer patients than that in experimental animals [85]. This is attributable to the fact that the level of tissue penetration of nanoparticles is often lower in the human tumor than in tumors experimentally induced in rodents. The latter is formed in a short duration (a few weeks) and thus have more leaky vessels as a result of excessive angiogenesis. It is likely that, although magnetic targeting increased the overall drug accumulation in the human tumor, only a fraction of cancer cells had drug molecules at a therapeutic level.

Magnetic targeting has been extensively explored for gene delivery. Indeed, the term, “magnetofection”, is coined for using a magnetic field to improve the transfection efficiency of genetic materials. There have been many reports on using magnetofection to achieve high

transfection efficiency in cultured cells, especially in the cells that are hard to transfect using conventional gene delivery methods. The MIONs designed for magnetofection are usually coated with cationic polymers, e.g., polyethylenimine (PEI), or cationic lipids for adsorption of siRNAs or DNA plasmids through electrostatic interactions [5,86]. The applied magnetic field can concentrate the MIONs on the cell surface, thereby enhancing cellular uptake of the nucleic acids they carry. After internalized by the cells, the cationic coating further destabilizes the endosomes to release the cargos into the cytoplasm. Magnetic targeting can also improve *in vivo* gene delivery. For example, siRNAs mixed with liposomes containing magnetic nanoparticles could be magnetically targeted to subcutaneous tumors in a mouse model, resulting in reduced tumor growth [5].

For *in vivo* delivery of large DNA plasmids, nanoparticle-mediated delivery often yields much lower gene expression than that of viral vectors. Viral vectors engineered from mammalian-derived viruses such as lentivirus, adenovirus, and adeno-associated virus (AAV), are naturally built nanoparticles with highly efficient machinery for transducing mammalian cells. Further, viral vectors administrated *in vivo* can disseminate via systemic circulation and replicate in specific organs following their tissue tropism [87]. The complexes of MIONs and viral particles can take advantage of the controllability of MIONs and the high transduction efficiency of viral vectors for targeted gene delivery. For example, MIONs can be attached to viral particles via electrostatic interaction or covalent conjugation, depending on the surface properties of the viral particles [8,86]. An applied magnetic field can drive the margination of magnetized viral vectors in the body fluids and increase their cell entry in the target tissue. This strategy is important for tissues that otherwise cannot be transduced efficiently. For example, the adenoviral vectors complexed with MIONs could transduce the fundic glands in the luminal surface of the stomach, in which the fluid with extreme pH and abundant digestive enzymes inhibits conventional gene delivery [86]. However, magnetic targeting will not alter the tissue tropism of viral vectors nor the amplification of delivered genes beyond the target tissue.

Recently, CRISPR/Cas9-mediated genome editing has shown great promise for treating genetic diseases [88,89]. The Cas9 nuclease coupled with guide RNAs (gRNAs) and in some cases DNA donor templates allows modification (insertion, mutation or deletion) of targeted D NA sequences, enabling the correction of disease-causing genes. The CRISPR/Cas9 system can be delivered as DNA plasmids packaged in a viral vector. However, the expression of the CRISPR/Cas9 gene editing machinery needs to be tightly regulated to avoid genotoxicity and immunogenicity [90,91]. A recent study showed that MIONs complexed with a baculoviral (BV) vector could be used to induce local and transient gene expression *in vivo* (Figure 4) [92]. Derived from an insect virus, *Autographs californica* multicapsid nucleopolyhedrovirus (AcMNPV), engineered BV vectors can efficiently transduce many types of mammalian cells and the transgene expression lasts only a few days in mammalian cells due to lack of replication capability [93]. Importantly, the complement system in the blood serum can inactivate BV vectors via enzymatic disruption [94]. However, when the BV particle is complexed with MIONs (MNP-BV) (Figure 4A), a magnetic field applied to the target tissue (Figure 4B) can help MNP-BV escape the inactivation by accelerating its cell entry, while the MNP-BV transduction is inhibited elsewhere (Figures 4C). Therefore, the interplay between the magnetic field and the

complement system facilitates local transgene expression of MNP-BV, making it a unique *in vivo* delivery platform for CRISPR/Cas9-mediated genome editing with spatial control (Figures 4D).

In recent years, cell-based therapies have emerged as a promising therapeutic approach for many diseases, including reprogramming stem cells for regenerative medicine and immune cells for cancer therapy. Similar to that of chemotherapy, the therapeutic effects of cell therapies rely on adequate recruitment of engineered cells to the target tissue, whereas the cells disseminated to normal tissue increase the risks of teratoma or autoimmune responses. Applications of magnetic targeting in cell therapies require the cells to be magnetized, usually by inducing cellular uptake of MIONs *in vitro*. Studies have shown that due to the small size of MIONs, more than 10^6 MIONs could be loaded into each human mesenchymal stem cell (hMSC) without compromising its viability and pluripotency [6,9]. After intravenous injection, these magnetized hMSCs could be captured in the tail vein or the femoral artery with small block magnets. Another study in a mouse tumor model further showed that macrophages containing MIONs could be directed to either the primary prostate tumor or the pulmonary metastasis under a magnetic field generated by a small animal MRI instrument, proving the feasibility of magnetic targeting inside the body (Figure 5) [7]. Magnetic targeting of oncolytic macrophages could significantly increase the area of necrosis in the primary tumor and reduce the count of pulmonary metastasis.

Taken together, magnetic targeting has been successfully demonstrated in cultured cells or with tumors in small animals, which involves either a single layer of cells or a small tissue volume that can be easily encompassed by the magnet field of small permanent magnets. Clinical studies suggest that magnetic targeting in the human body requires the computational design of the magnetic field that takes into account the arrangement of the magnets, the anatomical structure of the target tissue, and the pharmacokinetics of injected MIONs. The computational modeling indicates that magnetic targeting to tissues located a few centimeters under the skin can be realized by magnets with sizes comparable to that of a clinical MRI instrument, which presents a major technical challenge. One possible solution is the use of an magnetic particle imaging instrument that can generate a relatively focused magnetic field gradient [95,96]. Nevertheless, compared with the first generation of MIONs used in the clinical studies, high-quality MIONs can now be synthesized with better control of size distribution and coating, which helps balance the important parameters among the magnetic force, circulation profile and penetration depth in the tissue. Emerging medical fields such as cancer immunotherapy and therapeutic genome editing provide new opportunities for the application of magnetic targeting.

Diagnostic imaging and cell tracking

MIONs have been extensively studied as MRI contrast agents since the 1980s, and several forms of them approved for clinical diagnostic imaging (Table 2) [41,42]. In MRI, the hydrogen atoms, mostly water protons in the body fluids, are excited by a radio frequency pulse. Excited hydrogen atoms will return to the equilibrium state via two relaxation processes, longitudinal (spin-lattice) relaxation T_1 and transverse (spin-spin) relaxation T_2. The relaxation processes depend on the interaction of water molecules with nearby

biomolecules. This feature is used by many MRI techniques to delineate the tissue structure. MIONs distributed in the tissue can provide T_1 or T_2 contrast by generating a local magnetic field that alters the relaxation of water protons in the proximity. For most MIONs, T_2 contrast is dominant due to their gigantic magnetic moment. Here, MIONs accelerate the decay of the transverse magnetization of water protons, thereby generating a dark spot in T_2-weighted images. T_2 relaxivity or R_2 (= $1/T_2$) of MIONs increases with the magnetic moment of the crystalline core, which can be improved by increasing the core size or doping with other metal elements [32,97]. The coating of MIONs also influences the T_2 relaxation by limiting the access of water molecules to the core [98,99]. Thus, a larger crystalline core and a thinner coating lead to higher R_2. The first generation of MIONs synthesized via coprecipitation, e.g., Feridex I.V.® and Resovist®, often have an R_2 below or around 100 s^{-1} mM^{-1} Fe, whereas the R_2 of MIONs synthesized via thermodecomposition can be several folds higher with the same amount of Fe and several orders of magnitude higher on a per particle basis [98,100,101].

The most important application of MION-based imaging is the early detection and diagnosis of cancer. To date, tumor detection is realized via three distinct mechanisms underlying the biodistribution of MIONs. First, similar to most nanomaterials, MIONs administrated into the systemic circulation are rapidly captured by the macrophages in MPS that involves the liver, spleen, lymph nodes, and bone marrow [31,102]. The accumulation of MIONs in normal liver tissue will make the tissue appear dark in T_2-weighted images, whereas the liver tumor will stay as a bright spot because the lack of phagocytic activity in the tumor leads to low accumulation of MIONs. Likewise, normal lymph-nodes will become dark in T_2-weighted images and the occult lymph-nodes as a result of metastasis remain white and can be readily identified [42]. Clinical translation of these imaging applications started in the 1980s, which led to the approval of Feridex I.V.® and Resovist® in the U.S. and Europe respectively [103]. However, most clinical formulations have been discontinued due to the lack of financial interest and the competition from other contrast agents, in particular, gadolinium-based contrast agents [104].

In the organs not associated with MPS, the enhanced permeability and retention effect (EPR) in solid tumors plays an important role in the penetration of MIONs into tumor tissue. In normal tissues, the pore size on the vessel wall is less than 10 nm, which prevent most circulating macromolecules and nanomaterials from entering the interstitial space. In contrast, due to excessive and derailed angiogenesis in the tumor, the pore size on the tumor vessel wall can reach more than 100 nm depending on the type, location, and stage of the tumor [105–107]. In addition, solid tumors lack functional lymphatic vessels to help remove the macromolecules from the interstitial space. MIONs in the blood circulation can extravasate from the leaky tumor vessel wall and accumulate in the tumor tissue, thus generating a dark contrast in the tumor [34,108]. Further, MIONs can be conjugated with ligands that target tumor markers. Common tumor markers include VEGF receptors and $\alpha_v\beta_3$ integrins expressed by the endothelial cells in tumor vessels and folate receptors, transferrin receptors, and epidermal growth factor receptors upregulated on the surface of many cancer cells [32,109,110]. Accumulation of targeted MIONs in the tumor involves both passive targeting due to the EPR effect and active targeting via binding to the tumor markers, although the effectiveness of targeting remains debatable[111]. In addition to tumor

imaging, the use of MIONs has been explored for the detection of vascular abnormalities, inflammation, and cardiovascular diseases by either MR angiography or imaging molecular markers on the vessel surface [112].

The effectiveness of cell therapies relies on the trafficking and distribution of therapeutic cells in the body. For this reason, *in vivo* cell tracking is important for the design, evaluation, and monitoring of cell therapies. MRI is a preferred imaging modality for cell tracking because of its nonionizing nature, deep tissue imaging, and excellent soft tissue contrast. To generate MRI contrast, the cells of interest are often loaded with MIONs via either surface labeling or cellular uptake. Millions of MIONs can be loaded into each cell with the help of magnetofection, electroporation, or cell penetrating peptides [6,33,113]. Studies have shown that MIONs endocytosed by the cells will accumulate in the lysosomes for several days with negligible effects on the cell behaviors [6,114,115]. MION-facilitated cell tracking can achieve single cell detection *in vitro* [33,115]. Several studies have shown that the delivery of antigen-specific cytotoxic T-lymphocyte, natural killer cells, or dendritic cells to the tumor or regional lymph nodes could be monitored *in vivo* in real-time [113,115,116]. Further, real-time imaging of injected immune cells can provide critical information about the outcome of the treatment (Figure 6). Other than labeling cells *in vitro*, it has also been shown that MIONs administrated into the blood circulation could be taken up by circulating monocytes and tissue macrophages and recruited to inflammatory sites in the body. This strategy can be used to detect pathological processes involving inflammation such as atherosclerosis, pancreatic islet inflammation, or cardiac allograft rejection [117–119].

It should be noted that in clinical imaging applications, the dark T_2 contrast generated by MIONs is susceptible to the interference of background signals, voids in the body, and the artifacts caused by blood flow. Many efforts have been focused on developing MRI methods that utilize MIONs as positive (bright) contrast agents [120–122]. In particular, as the size of MIONs decreases, the T_1 effect of MIONs can be detected using proper MRI sequences, and MIONs with core sizes less than 5 nm can generate a high T_1 contrast [123,124]. Thanks to the superior biocompatibility, MION-based T_1 contrast agents are potential substitutes for gadolinium compounds in clinical MRI. In addition, a new imaging technique, magnetic particle imaging (MPI), the first imaging technique built specifically for nanoparticle-based contrast agents, has been developed based on the detection of the nonlinear magnetic response of MIONs in an oscillating magnetic field [95,125]. The high sensitivity and fast imaging time of MPI are very attractive for examining the biodistribution of MIONs in the body, and the commercialization of the MPI instrument will accelerate the exploration of its full potential.

Magnetic nanoparticle hyperthermia

Hyperthermia therapy often refers to the application of heat as an adjunct therapy for cancer treatment. The effects of hyperthermia are linked to the heat shock responses and physiological changes induced by elevated temperature in the tumor tissue [126]. Numerous clinical studies have demonstrated that hyperthermia can improve the efficacy of radiation therapy, chemotherapy, and immunotherapy of many types of cancers [127,128]. The clinical significance of hyperthermia has prompted an extensive search for thermal techniques that

can heat the tissue more efficiently. It is known that magnetic materials exposed to an alternating magnetic field (AMF) can convert electromagnetic energy into thermal energy. Investigation of MION-induced heating for cancer treatment, i.e., magnetic nanoparticle hyperthermia, started in the 1980s [129–131]. Magnetic nanoparticle hyperthermia is also known as magnetic hyperthermia, magnetic nanoparticle heating, or magnetic fluid heating among others. Note that heating the tissue above 45°C leads to tissue necrosis and is commonly referred to as thermal ablation, whereas hyperthermia often means heating the tissue to a temperature of 41~45°C. For simplicity, we will use the term, magnetic nanoparticle hyperthermia, for all MION-mediated cancer thermal therapies. To date, magnetic nanoparticle hyperthermia has received EMA approval for the treatment of glioblastoma multiforme in Germany under the brand of NanoTherm® (Table 2) [37]. A clinical trial of NanoTherm® for the treatment of intermediate-risk prostate cancer has been approved in the United States. In addition, MION-induced heating has shown its potential in areas such as combination cancer therapy, organ preservation, controlled drug delivery, and magnetogenetics.

Heat generation of MIONs in an AMF is the result of their magnetic relaxation in response to the field change. The heating efficiency of MIONs, measured by specific absorption rate (SAR), depends on several features of MIONs, including the magnetic susceptibility, magnetic anisotropy, and the size of the iron oxide cores. SAR also increases with the field strength (H) and frequency (f) of the AMF. However, building an inductive coil that generates an AMF of high strength and high frequency for a human body is both technically challenging and costly [132]. The AMF of high frequency ($f > 10^6$ Hz) can also induce eddy currents in the body fluid, which lead to nonspecific heating of the tissue. A safety limit, $H.f \times 5\times10^9$ $Am^{-1}S^{-1}$, is empirically imposed on the AMF in clinical applications [58,129]. The optimal range of the field strength and frequency of the AMF is on the order of 10 kA/m and 100 kHz respectively. For this reason, the current effort on increasing the heating efficiency is mainly directed toward optimizing the properties of MIONs.

A number of studies have been focused on elucidating the mechanisms underlying magnetic nanoparticle hyperthermia. In a well-known study, Rosensweig modeled the heat generation in magnetic nanoparticle hyperthermia as the energy conversion during the magnetic relaxation of nanoparticles in a cyclic magnetic field [133]. Based on the assumptions that the nanoparticles have a uniaxial symmetry and respond linearly to the field change, an analytic solution of SAR was derived as,

$$SAR = \pi\mu_0\chi_0 H_0^2 f \frac{2\pi f\tau}{1+(2\pi f\tau)^2} \quad (2)$$

where μ_0 is the magnetic permeability of vacuum, χ_0 is the equilibrium susceptibility, and τ is the relaxation time of MIONs determined by two size-dependent processes, Néel relaxation and rotational Brownian motion, represented by τ_N and τ_B respectively ($1/\tau = 1/\tau_N + 1/\tau_B$). This model predicts that the highest heating efficiency can be reached if $2\pi f\tau$ equals to 1. As such, the heating efficiency of MIONs would peak at a size of 14 nm in an AMF of 300 kHz[133]. Although the size-dependence predicted by the Rosensweig-model was confirmed experimentally [21,134,135], several recent studies showed that the SAR of

MIONs increases monotonically with size [12,136,137]. The discrepancy in experimental measurements is likely due to the differences in the dispersity of MIONs in the medium, size distribution (especially non-uniformity) and the crystal structure of MIONs arising from different synthesis methods [138]. Nevertheless, the uniaxial magnetic anisotropy and linear response assumptions cannot accurately model magnetite nanocrystals, which have a face-centered cubic lattice. Several other models have been proposed to better predict the heating efficiency of MIONs [12,58,139].

Compared with other clinical thermal techniques, magnetic nanoparticle hyperthermia has several advantages [140]. First, the absorption and scattering of the AMF by biological tissues are negligible. Magnetic nanoparticle hyperthermia can thus heat the tissue deep inside the body, as in the case of intracranial heating by NanoTherm®, without causing adverse effects. Secondly, in magnetic nanoparticle hyperthermia, the region of heating is determined by the spatial distribution of MIONs and the AMF, thus facilitating highly localized and efficient heating inside the tumor via targeted delivery of MIONs and proper placement of the inductive coil. The tumor tissue under magnetic nanoparticle hyperthermia can be heated to 50°C without causing collateral tissue/organ damage [37]. Lastly, MIONs can serve as MRI contrast agents, so the distribution and concentration of MIONs in the body can be assessed with MRI to help tailor the thermal dose in the treatment [141]. On the other hand, compared with other thermal techniques, such as focused ultrasound, radiofrequency heating, and gold nanomaterial-mediated heating, the heating efficiency of magnetic nanoparticle hyperthermia is considerably lower [142]. The concentration of MIONs in the tissue needs to reach milligram per milliliter range to generate adequate heating, which often requires intratumoral injection of MIONs. Recent studies have shown that MIONs can be heated efficiently by a near infrared laser, which may provide a more biocompatible alternative to the gold nanomaterial-based photothermal therapy [143] (More details can be found in ref [142]).

Thermal ablation of local tumors with magnetic nanoparticle hyperthermia has shown great promise in reducing disease progression, which is a less invasive alternative to surgical removal of the tumor mass. In particular, it provides a valuable therapeutic option for non-resectable tumors, including the tumors in certain locations in the brain, lung, liver, and pancreas. In a clinical study of NanoTherm® treatment of recurrent glioblastoma, MIONs were administrated into the tumor via intracranial injection and the tumor was heated to 50°C (Figure 7) [37], and patients treated by NanoTherm® and adjunct radiation therapy had an overall survival of 23.2 months compared to 14.6 months in the reference group [37]. In preclinical and clinical studies, local tumor ablation via magnetic nanoparticle hyperthermia has also been investigated for liver cancer, esophageal cancer, pancreatic cancer, and prostate cancer [144,145].

Mild hyperthermia (41~43 °C) is known to trigger the differentiation of cancer cells and sensitize fast-dividing cancer cells to other treatment such as chemotherapy and radiation [40,128]. Previous studies have found that MIONs loaded with doxorubicin had higher *in vitro* cytotoxicity on m ultidrug-resistant human ovarian carcinoma cells (A2780/AD) and human cervical cancer cells (HeLa) under an AMF, presumably due to the synergistic effect of hyperthermia and chemotherapy [146,147]. Importantly, emerged as a new frontier of

cancer treatment in the past few years, cancer immunotherapy seeks to induce or enhance immune responses against tumor cells, thereby fighting cancer with the patient's own immune system. Many preclinical and clinical studies have shown that combination therapies that modulate different aspects of anti-cancer immunity can significantly improve the therapeutic outcome [148]. The regulation of body temperature is inherently connected with the immunological responses in the body [149]. It is thus intuitive to benefit from the synergy between hyperthermia and cancer immunotherapy. Ito, et al. showed that local magnetic hyperthermia followed by intratumoral injection of interleukin-2 (IL-2) or granulocyte macrophage-colony stimulating factor (GM-CSF) in a mouse B16 melanoma model could lead to tumor remission due to increased anti-tumor immunity generated by heating-induced cell death in addition to that of injected cytokines [150]. Local hyperthermia-mediated immune stimulation can circumvent the adverse effects associated with systemically administrated immunotherapies since nanoparticle heating is limited to the tumor tissue. It is anticipated that magnetic nanoparticle hyperthermia will find many applications in enhancing cancer immunotherapy as we gain a better understanding of the interplay between hyperthermia and immunological processes in the tumor microenvironment. It should be noted that MIONs can generate reactive oxygen species (ROS) via Fenton reaction, which is enhanced under magnetic heating [151,152]. While more studies are needed to distinguish the biological effects of thermal stress from those of ROS, these findings reveal new therapeutic potential of magnetic nanoparticles hyperthermia.

MION-induced heating may also address an important issue in organ transplantation. Currently, organ transplantation requires immediate delivery of the harvested organ from the donor to the patient because most organs cannot be preserved functionally beyond a few hours [153]. It is known that the biological tissues with proper cryoprotection can be stored in liquid nitrogen for many years. However, for large tissues or organs, the convection-based thawing process will generate large thermal stresses that lead to inferior tissue viability due to heterogeneous heating. Tissue thawing after cryopreservation is, therefore, the major bottleneck in organ transplantation. A potential solution is to infuse the tissue/organ with the cryoprotectant containing MIONs before freezing and, right before transplantation, to perform tissue thawing by heating the MIONs with an AMF. Compared with other thermal techniques, this approach provides more homogeneous heating throughout the tissue [154]. Manuchehrabadi, et al. demonstrated this strategy using MIONs with 12 nm cores and a mesoporous silica coating [36], and showed that it significantly improved the viability of the porcine carotid artery compared with the gold standard convective warming. However, extending this new tissue-thawing method to larger tissues/organs requires further improvement of the heating efficiency and the AMF generator.

Although MIONs can heat tissues or organs effectively under AMF, there have been many debates over their capability of microscopic heating. The classical Fourier heat conduction therapy indicates that heat dissipation is proportional to the surface area, whereas heat generation is proportional to the volume. Accordingly, given the typical heating efficiency of MIONs, it was predicted that the region occupied by MIONs needs to be at least 1.1 mm in diameter in order to have effective focal heating [155]. Conversely, Chen suggested that the temperature increase due to MIONs could be much higher than that predicted with the

Fourier theory due to the nonlocal and nonequilibrium nature of the heat transfer at the nanoscale [156], making it possible to heat the molecules in the vicinity of a single MION. Huang et al. first demonstrated the feasibility of molecular (nanoscale) heating of a temperature-sensing protein, transient receptor potential vanilloid 1 (TRPV1) [38]. They showed that the MION bound to TRPV1 could generate sufficient heat to trigger the opening of TRPV1 channels despite the moderate temperature increase in the solution. Importantly, the thermal activation of TRPV1 could trigger action potentials in cultured hippocampal neurons. Furthermore, in *in vivo* settings, MION-induced local heat could stimulate neurons transduced by the viral vectors encoding TRPV1 genes in the deep brain (Figure 8) [157,158]. Magnetic stimulation of TRPV1, referred to as magnetogenetics, provides one of a handful of methods for investigating brain functions, which may have significant implications for neuroscience. Similarly, Stanley et al. showed that ferritin nanoparticles, i.e. biosynthesized MIONs, could be utilized to regulate glucose homeostasis, also via stimulation of TRPV1, in genetically modified mice [35,64]. In addition, it has been shown that the MIONs accumulated in the lysosomes could generate sufficient heat to permeabilize the lysosome membrane and induce cell death without causing a detectable temperature rise in the environment [159]. MIONs can thus be used to kill cancer cells via targeted heating of the lysosomes in the cancer cells [160]. A similar application is magnetically triggered drug release from microcapsules, polymersomes or liposomes, in which the MIONs embedded in the membrane disrupts the thermosensitive membrane via magnetic heating [161–163]. This evidence suggests that MIONs can serve as a point heat source to activate the molecules in close proximity. Although the physics of energy transfer at the molecular level is not fully understood, molecular heating opens up new opportunities in areas from basic research to therapeutic interventions.

Concluding remarks

The nanomagnetism that allows the generation of local magnetic, mechanical, and thermal fields around individual cells or molecules has provided unique tools for biomedical research and clinical applications. Advances in MIONs are driven by both our ability to fabricate MIONs with better properties and the needs of biomedical applications. The first generation of MIONs consists of small nanocrystals (< 10 nm) synthesized via coprecipitation. The size range of the nanocrystals has increased to tens of nanometers via thermodecomposition and to hundreds of nanometers via the formation of nanoclusters. The increase in size gives rise to orders of magnitude increase in the magnetic force, imaging contrast, and magnetic heating efficiency, which become biologically relevant at the molecular and cellular levels. Concurrently, in modern medicine, the “one size fits all” therapies are gradually replaced by precision medicine that aims to target specific disease-causing molecules or cells based on personalized diagnosis. The development in both fields helps extend the applications of MIONs from conventional drug delivery, imaging, and hyperthermia to genome editing, cell therapy, and neuroscience.

There are many important issues remaining to be addressed. For example, there is a need to elucidate the mechanisms of heat generation, energy transfer and inter-particle interaction at the nanoscale, which requires a collective effort at the interface of material science, quantum mechanics, and chemistry. Further, the biological functions of MIONs rely on their ability to

reach the target molecules/cells *in vivo*. Developing new strategies that overcome *in vivo* transport barriers from the systemic to the cellular level is critically needed. It requires not only novel nanofabrication techniques but also a better understanding of the nano-bio interactions, including immunological responses toward nanomaterials. Another important issue is that the clinical translation of MION-based technologies often relies on the generation of a relevant electromagnetic field inside the body. The development of NanoActivator® for NanoTherm® as well as commercialization of the small animal MPI instrument are good examples. Extensive efforts are required to push more applications of MIONs into the clinics. As we move forward in this multidisciplinary field, there will be more MION-based molecular therapeutics emerging in the next decade.

Acknowledgments

This work was supported by the Cancer Prevention and Research Institute of Texas (RR140081 to G.B.) and the National Institutes of Health (R01EB026893 to S.T.).

References

1. Widder KJ, et al., Proc Soc Exp Biol Med (1978) 158 (2), 141 [PubMed: 674215]
2. Ranney DF, Science (1985) 227 (4683), 182 [PubMed: 3966151]
3. Widder KJ, et al., Proc Natl Acad Sci U S A (1981) 78 (1), 579 [PubMed: 6941258]
4. Alexiou C, et al., Cancer Res (2000) 60 (23), 6641 [PubMed: 11118047]
5. Namiki Y, et al., Nat Nanotechnol (2009) 4 (9), 598 [PubMed: 19734934]
6. Landazuri N, et al., Small (2013) 9 (23), 4017 [PubMed: 23766267]
7. Muthana M, et al., Nat Commun (2015) 6, 8009 [PubMed: 26284300]
8. Hofmann A, et al., Proc Natl Acad Sci U S A (2009) 106 (1), 44 [PubMed: 19118196]
9. Riegler J, et al., Biomaterials (2013) 34 (8), 1987 [PubMed: 23237516]
10. Krishnan KM, et al., J Mater Sci (2006) 41 (3), 793
11. Yanes R, et al., Phys Rev B (2007) 76 (6)
12. Tong S, et al., ACS Nano (2017) 11 (7), 6808 [PubMed: 28625045]
13. Demortiere A, et al., Nanoscale (2011) 3 (1), 225 [PubMed: 21060937]
14. Jun YW, et al., Journal of the American Chemical Society (2005) 127 (16), 5732 [PubMed: 15839639]
15. Jana NR, et al., Chem Mater (2004) 16 (20), 3931
16. Sun S, et al., J Am Chem Soc (2004) 126 (1), 273 [PubMed: 14709092]
17. Park J, et al., Nat Mater (2004) 3 (12), 891 [PubMed: 15568032]
18. Park J, et al., Angew Chem Int Ed Engl (2005) 44 (19), 2873 [PubMed: 15798989]
19. Ge J, et al., Angew Chem Int Ed Engl (2007) 46 (23), 4342 [PubMed: 17465432]
20. Zhao Z, et al., Nat Commun (2013) 4, 2266 [PubMed: 23903002]
21. Lee JH, et al., Nat Nanotechnol (2011) 6 (7), 418 [PubMed: 21706024]
22. Usov NA, et al., J Supercond Nov Magn (2013) 26 (4), 1079
23. Furlani EP, and Ng KC, Phys Rev E Stat Nonlin Soft Matter Phys (2008) 77 (6 Pt 1), 061914 [PubMed: 18643307]
24. Plank C, et al., J Liposome Res (2003) 13 (1), 29 [PubMed: 12725725]
25. Etoc F, et al., Nano Lett (2015) 15 (5), 3487 [PubMed: 25895433]
26. Dobson J, Nat Nanotechnol (2008) 3 (3), 139 [PubMed: 18654485]
27. Qiu Y, et al., Nat Commun (2017) 8, 15594 [PubMed: 28593939]
28. Hu B, et al., Nanomed-Nanotechnol (2014) 10 (1), 45
29. Mannix RJ, et al., Nat Nanotechnol (2008) 3 (1), 36 [PubMed: 18654448]

30. Du V, et al., Nat Commun (2017) 8 (1), 400 [PubMed: 28900152]
31. Weissleder R, et al., Radiology (1990) 175 (2), 489 [PubMed: 2326474]
32. Lee JH, et al., Nat Med (2007) 13 (1), 95 [PubMed: 17187073]
33. Lewin M, et al., Nat Biotechnol (2000) 18 (4), 410 [PubMed: 10748521]
34. Kircher MF, et al., Cancer Res (2003) 63 (23), 8122 [PubMed: 14678964]
35. Stanley SA, et al., Science (2012) 336 (6081), 604 [PubMed: 22556257]
36. Manuchehrabadi N, et al., Science translational medicine (2017) 9 (379)
37. Maier-Hauff K, et al., J Neurooncol (2011) 103 (2), 317 [PubMed: 20845061]
38. Huang H, et al., Nat Nanotechnol (2010) 5 (8), 602 [PubMed: 20581833]
39. Leibiger IB, and Berggren PO, Nat Med (2015) 21 (1), 14 [PubMed: 25569545]
40. Moise S, et al., Nanoscale (2018) 10 (44), 20519 [PubMed: 30397703]
41. Wang YX, et al., Eur Radiol (2001) 11 (11), 2319 [PubMed: 11702180]
42. Harisinghani MG, et al., N Engl J Med (2003) 348 (25), 2491 [PubMed: 12815134]
43. Guardia P, et al., J Phys Chem C (2011) 115 (2), 390
44. Albanese A, et al., Annu Rev Biomed Eng (2012) 14, 1 [PubMed: 22524388]
45. Laurent S, et al., Chem Rev (2008) 108 (6), 2064 [PubMed: 18543879]
46. Clement O, et al., Top Magn Reson Imaging (1998) 9 (3), 167 [PubMed: 9621405]
47. Reynolds F, et al., Analytical Chemistry (2005) 77 (3), 814 [PubMed: 15679348]
48. Yu WW, et al., Nanotechnology (2006) 17 (17), 4483
49. Murray CB, et al., Annu Rev Mater Sci (2000) 30, 545
50. Peng XG, et al., Journal of the American Chemical Society (1998) 120 (21), 5343
51. Vreeland EC, et al., Chem Mater (2015) 27 (17), 6059
52. Kim D, et al., J Am Chem Soc (2009) 131 (2), 454 [PubMed: 19099480]
53. Qiao L, et al., ACS Nano (2017) 11 (6), 6370 [PubMed: 28599110]
54. Vasanawala SS, et al., Magn Reson Med (2016) 75 (5), 2107 [PubMed: 26890830]
55. Jang JT, et al., Angewandte Chemie-International Edition (2009) 48 (7), 1234 [PubMed: 19137514]
56. Philipse AP, and Maas D, Langmuir (2002) 18 (25), 9977
57. Hergt R, et al., J Magn Magn Mater (2005) 293 (1), 80
58. Hergt R, and Dutz S, J Magn Magn Mater (2007) 311 (1), 187
59. Zurkiya O, et al., Magnet Reson Med (2008) 59 (6), 1225
60. Elfick A, et al., Scientific reports (2017) 7, 39755 [PubMed: 28051139]
61. Kerans FFA, et al., International journal of molecular sciences (2018) 19 (10)
62. Van de Walle A, et al., Proc Natl Acad Sci U S A (2019)
63. Genove G, et al., Nat Med (2005) 11 (4), 450 [PubMed: 15778721]
64. Stanley SA, et al., Nat Med (2015) 21 (1), 92 [PubMed: 25501906]
65. Montet X, et al., J Med Chem (2006) 49 (20), 6087 [PubMed: 17004722]
66. Xie J, et al., Advanced Materials (2007) 19 (20), 3163
67. Lattuada M, and Hatton TA, Langmuir (2007) 23 (4), 2158 [PubMed: 17279708]
68. Qu H, et al., Langmuir (2011) 27 (6), 2271 [PubMed: 21284390]
69. Tong S, et al., Nano Lett (2011) 11 (9), 3720 [PubMed: 21793503]
70. Kim J, et al., Angew Chem Int Ed Engl (2008) 47 (44), 8438 [PubMed: 18726979]
71. Kim Y, et al., Nano Lett (2012) 12 (7), 3587 [PubMed: 22716029]
72. Xie J, et al., Biomaterials (2010) 31 (11), 3016 [PubMed: 20092887]
73. Herbst RS, et al., Lancet (2016) 387 (10027), 1540 [PubMed: 26712084]
74. Walkey CD, et al., J Am Chem Soc (2012) 134 (4), 2139 [PubMed: 22191645]
75. Walkey CD, et al., ACS Nano (2014) 8 (3), 2439 [PubMed: 24517450]
76. Weissleder R, et al., Advanced Drug Delivery Reviews (1995) 16 (2-3), 321

77. Furlani EP, and Ng KC, Phys Rev E Stat Nonlin Soft Matter Phys (2006) 73 (6 Pt 1), 061919 [PubMed: 16906876]
78. Earnshaw S, Trans. Camb. Phil. Soc (1842) 7, 97
79. Nacev A, et al., Nano Lett (2014)
80. Shapiro B, J Magn Magn Mater (2009) 321 (10), 1594 [PubMed: 20165553]
81. Lubbe AS, et al., Cancer Res (1996) 56 (20), 4694 [PubMed: 8840986]
82. Alexiou C, et al., J Drug Target (2003) 11 (3), 139 [PubMed: 13129824]
83. Lubbe AS, et al., Cancer Res (1996) 56 (20), 4686 [PubMed: 8840985]
84. Wilson MW, et al., Radiology (2004) 230 (1), 287 [PubMed: 14695402]
85. Soloman R, and Gabizon AA, Clin Lymphoma Myeloma (2008) 8 (1), 21 [PubMed: 18501085]
86. Scherer F, et al., Gene Ther (2002) 9 (2), 102 [PubMed: 11857068]
87. Wang Y, et al., Biotechniques (2005) 39 (6), 834 [PubMed: 16382900]
88. Sander JD, and Joung JK, Nat Biotechnol (2014) 32 (4), 347 [PubMed: 24584096]
89. Cox DB, et al., Nat Med (2015) 21 (2), 121 [PubMed: 25654603]
90. Hsu PD, et al., Nat Biotechnol (2013) 31 (9), 827 [PubMed: 23873081]
91. Lin YN, et al., Nucleic Acids Res (2014) 42 (11), 7473 [PubMed: 24838573]
92. Zhu H, et al., Nat Biomed Eng (2019) 3 (2), 126 [PubMed: 30944431]
93. Mansouri M, et al., Nat Commun (2016) 7, 11529 [PubMed: 27143231]
94. Hofmann C, and Strauss M, Gene Ther (1998) 5 (4), 531 [PubMed: 9614578]
95. Goodwill PW, et al., Adv Mater (2012) 24 (28), 3870 [PubMed: 22988557]
96. Griese F, et al., I S Biomed Imaging (2018), 1293
97. Tromsdorf UI, et al., Nano Lett (2007) 7 (8), 2422 [PubMed: 17658761]
98. Tong S, et al., Nano Lett (2010) 10 (11), 4607 [PubMed: 20939602]
99. LaConte LE, et al., J Magn Reson Imaging (2007) 26, 1634 [PubMed: 17968941]
100. Rohrer M, et al., Invest Radiol (2005) 40 (11), 715 [PubMed: 16230904]
101. Lee N, et al., Nano Lett (2012) 12 (6), 3127 [PubMed: 22575047]
102. Weissleder R, et al., AJR Am J Roentgenol (1989) 152 (1), 167 [PubMed: 2783272]
103. Seneterre E, et al., Radiology (1996) 200 (3), 785 [PubMed: 8756932]
104. Wang YX, Quantitative imaging in medicine and surgery (2011) 1 (1), 35 [PubMed: 23256052]
105. Carmeliet P, and Jain RK, Nature (2000) 407 (6801), 249 [PubMed: 11001068]
106. Yuan F, et al., Cancer Res (1995) 55 (17), 3752 [PubMed: 7641188]
107. Hobbs SK, et al., Proc Natl Acad Sci U S A (1998) 95 (8), 4607 [PubMed: 9539785]
108. Jain RK, and Stylianopoulos T, Nature reviews. Clinical oncology (2010) 7 (11), 653
109. Montet X, et al., Neoplasia (2006) 8 (3), 214 [PubMed: 16611415]
110. Kessinger CW, et al., Theranostics (2011) 1,263 [PubMed: 21562632]
111. Wilhelm S, et al., Nature Reviews Materials (2016) 1, 16014
112. Nahrendorf M, et al., Circulation (2006) 114 (14), 1504 [PubMed: 17000904]
113. Daldrup-Link HE, et al., Eur Radiol (2005) 15 (1), 4 [PubMed: 15616814]
114. Thu MS, et al., Nat Med (2012) 18 (3), 463 [PubMed: 22366951]
115. Kircher MF, et al., Cancer Res (2003) 63 (20), 6838 [PubMed: 14583481]
116. de Vries IJ, et al., Nat Biotechnol (2005) 23 (11), 1407 [PubMed: 16258544]
117. Kanno S, et al., Circulation (2001) 104 (8), 934 [PubMed: 11514382]
118. Denis MC, et al., Proc Natl Acad Sci U S A (2004) 101 (34), 12634 [PubMed: 15304647]
119. Kooi ME, et al., Circulation (2003) 107 (19), 2453 [PubMed: 12719280]
120. Seppenwoolde JH, et al., Magn Reson Med (2003) 50 (4), 784 [PubMed: 14523965]
121. Cunningham CH, et al., Magn Reson Med (2005) 53 (5), 999 [PubMed: 15844142]
122. Zurkiya O, and Hu XP, Magnet Reson Med (2006) 56 (4), 726
123. Kim BH, et al., J Am Chem Soc (2011) 133 (32), 12624 [PubMed: 21744804]
124. Wei H, et al., P Natl Acad Sci USA (2017) 114 (9), 2325

125. Gleich B, and Weizenecker J, Nature (2005) 435 (7046), 1214 [PubMed: 15988521]
126. Hildebrandt B, et al., Crit Rev Oncol Hematol (2002) 43 (1), 33 [PubMed: 12098606]
127. Mallory M, et al., Crit Rev Oncol Hematol (2016) 97, 56 [PubMed: 26315383]
128. Wust P, et al., Lancet Oncol (2002) 3 (8), 487 [PubMed: 12147435]
129. Brezovich IA, Medical physics monograph (1988) 16, 82
130. Jordan A, et al., Int J Hyperthermia (1993) 9 (1), 51 [PubMed: 8433026]
131. Sako M, et al., Nihon Gan Chiryo Gakkai Shi (1984) 19 (9), 2168 [PubMed: 6085107]
132. Christiansen MG, et al., The Review of scientific instruments (2017) 88 (8), 084301 [PubMed: 28863666]
133. Rosensweig RE, J Magn Magn Mater (2002) 252 (1-3), 370
134. Chen R, et al., ACS Nano (2013) 7 (10), 8990 [PubMed: 24016039]
135. Guardia P, et al., ACS Nano (2012) 6 (4), 3080 [PubMed: 22494015]
136. Guardia P, et al., J Mater Chem B (2014) 2 (28), 4426 [PubMed: 32261543]
137. Lartigue L, et al., J Am Chem Soc (2011) 133 (27), 10459 [PubMed: 21604803]
138. Nedelkoski Z, et al., Scientific reports (2017) 7, 45997 [PubMed: 28393876]
139. Carrey J, et al., J Appl Phys (2011) 109 (8), 083921
140. Moroz P, et al., Int J Hyperthermia (2002) 18 (4), 267 [PubMed: 12079583]
141. Zhang J, et al., Magn Reson Med (2017) 78 (2), 702 [PubMed: 27667655]
142. Espinosa A, et al., Advanced Functional Materials (2018) 28 (37)
143. Plan Sangnier A, et al., J Control Release (2018) 279, 271 [PubMed: 29684497]
144. Johannsen M, et al., Eur Urol (2007) 52 (6), 1653 [PubMed: 17125906]
145. Jones SK, et al., Int J Hyperthermia (2002) 18 (2), 117 [PubMed: 11911482]
146. Toraya-Brown S, and Fiering S, Int J Hyperthermia (2014) 30 (8), 531 [PubMed: 25430985]
147. Quinto CA, et al., Nanoscale (2015) 7 (29), 12728 [PubMed: 26154916]
148. Mahoney KM, et al., Nat Rev Drug Discov (2015) 14 (8), 561 [PubMed: 26228759]
149. Evans SS, et al., Nature reviews. Immunology (2015) 15 (6), 335
150. Ito A, et al., Cancer Sci (2003) 94 (3), 308 [PubMed: 12824927]
151. Gao L, et al., Nat Nanotechnol (2007) 2 (9), 577 [PubMed: 18654371]
152. Clerc P, et al., J Control Release (2018) 270, 120 [PubMed: 29203413]
153. Lewis JK, et al., Cryobiology (2016) 72 (2), 169 [PubMed: 26687388]
154. Etheridge ML, et al., TECHNOLOGY (2014) 02 (03), 229
155. Rabin Y, Int J Hyperthermia (2002) 18 (3), 194 [PubMed: 12028637]
156. Chen G, J Heat Trans-T Asme (1996) 118 (3), 539
157. Munshi R, et al., Elife (2017) 6
158. Chen R, et al., Science (2015) 347 (6229), 1477 [PubMed: 25765068]
159. Domenech M, et al., ACS Nano (2013) 7 (6), 5091 [PubMed: 23705969]
160. Creixell M, et al., ACS Nano (2011) 5 (9), 7124 [PubMed: 21838221]
161. Sanson C, et al., ACS Nano (2011) 5 (2), 1122 [PubMed: 21218795]
162. Carregal-Romero S, et al., Nanoscale (2015) 7 (2), 570 [PubMed: 25415565]
163. Katagiri K, et al., Small (2011) 7 (12), 1683 [PubMed: 21567941]

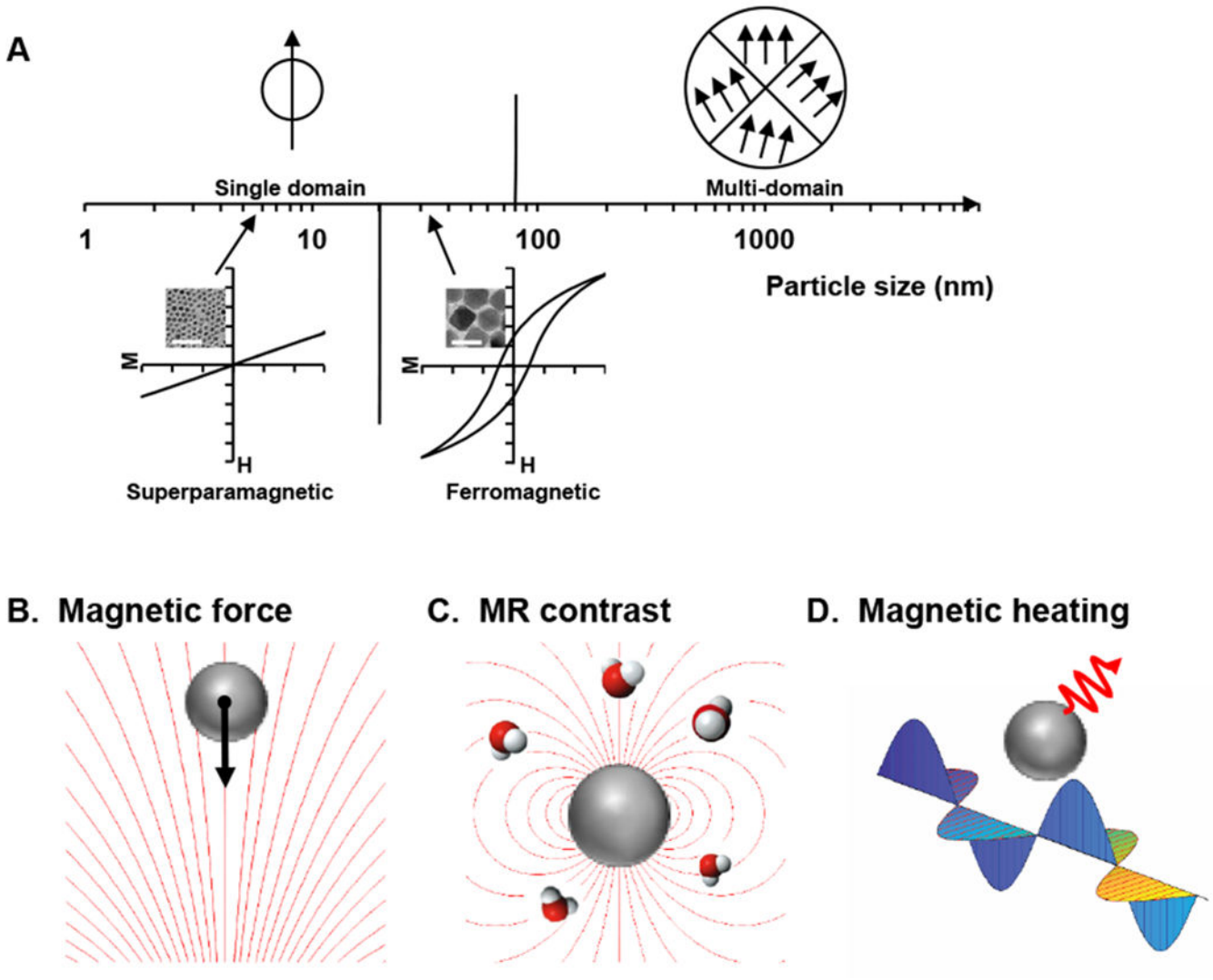

Figure 1. Properties of MIONs.

A. Size dependence of MIONs. MIONs change from multi-magnetic domain to single domain at 80 ~ 90 nm and from ferromagnetic to superparamagnetic at ~ 20 nm. Inserts are TEM images and hysteresis curves of 6 nm and 33 nm MIONs respectively. Scale bars equal 50 nm. Magnetic hysteresis was scanned from −300 Oe to 300 Oe by a superconducting quantum interference device (SQUID). (Reproduced with permission from [12], © 2017 American Chemical Society.) **B, C,** and **D** illustrate the three main magnetic properties of MIONs used in biomedical applications. **B**. Magnetic force generated by the interaction of MIONs with a nonuniform magnetic field. **C**. MR contrast due to the effect of MIONs on the relaxation of water protons. **D**. Magnetic heating generated by MIONs in an alternating magnetic field.

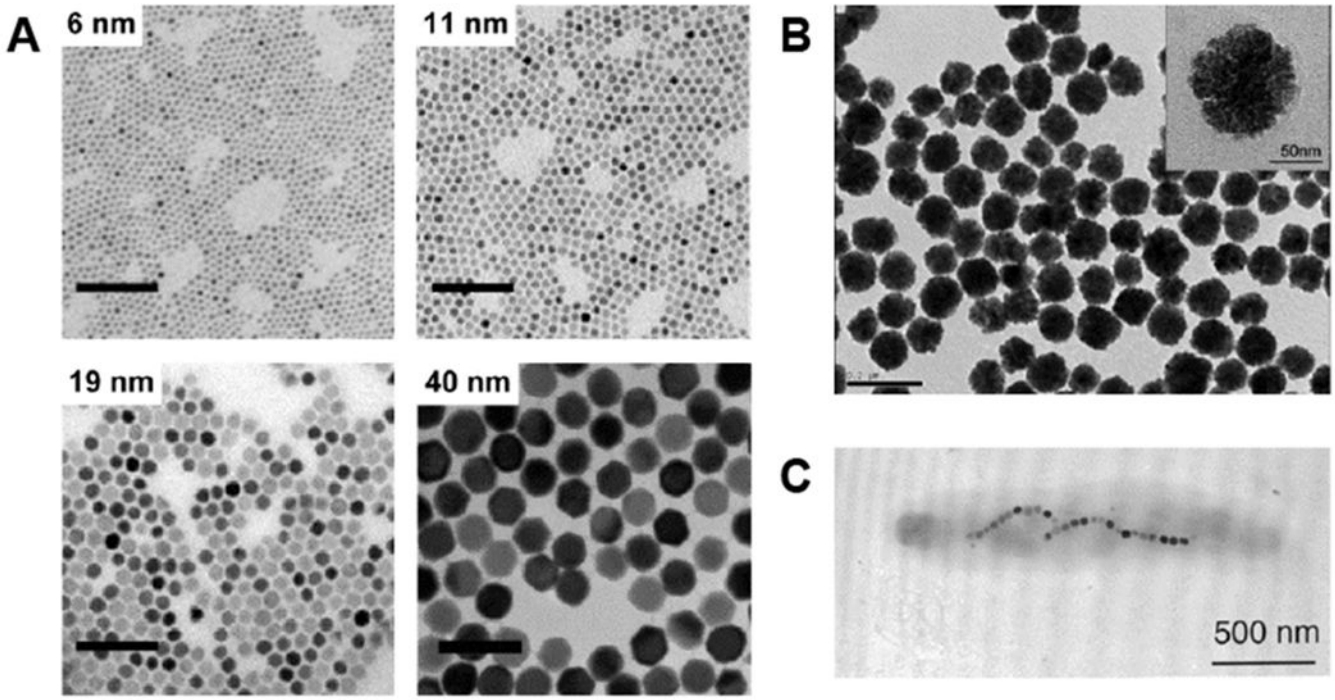

Figure 2. Synthesis of MIONs.

A. TEM images of MIONs synthesized via thermodecomposition of $Fe(acac)_3$. Scale bars equal 100 nm. (Reproduced with permission from [12], © 2017 American Chemical Society.) **B**. TEM image of nanoclusters formed of small magnetite nanocrystals crosslinked by poly(acrylic acid). The mean diameter of the nanoclusters is 93 nm. Insert shows the high-resolution image of a nanocluster. (Reproduced with permission from [19], © 2007 Wiley-VCH Verlag GmbH & Co. KGaA, Weinheim.) **C**. TEM image of a magnetotactic bacterium (M. magnetotacticum). The bacterium contains magnetite particles aligned in a chain parallel to its long axis. (Reproduced with permission from [56], © 2002 American Chemical Society.)

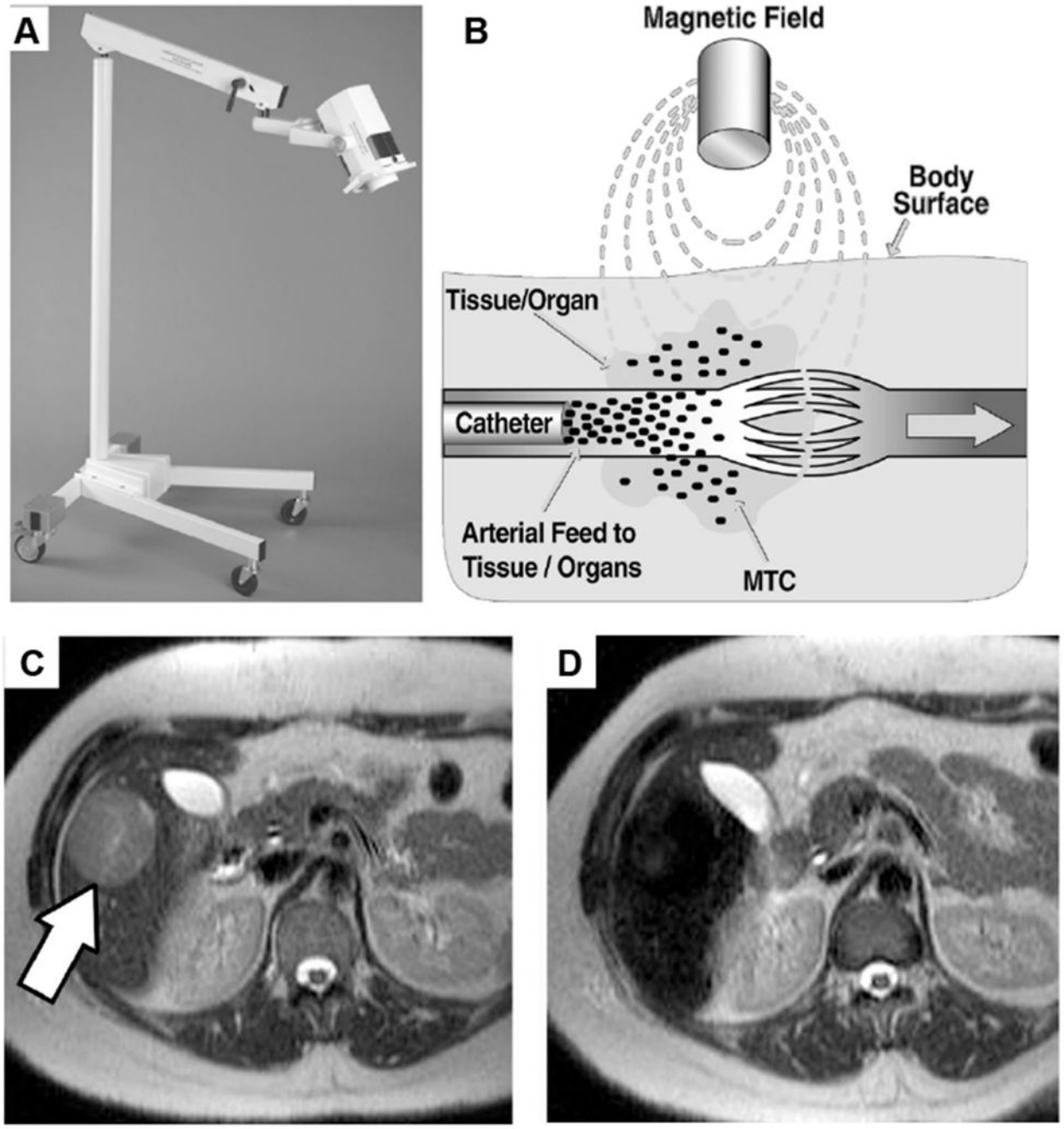

Figure 3. Magnetic targeted therapy.

A. The portable magnet used for magnetic targeted therapy. **B**. Diagram of magnetic targeted therapy. MTC-DOX (MTC) is infused into the tumor with a catheter inserted into the tumor feeding artery. (Image courtesy of FeRx.) **C** and **D** Transverse single-shot spin-echo MR images of a patient before and after magnetic targeted therapy. The tumor (arrow) in the right hepatic lobe turned dark because of the accumulation of MTC-DOX. (Reproduced with permission from [84], © 2004 The Radiological Society of North America.)

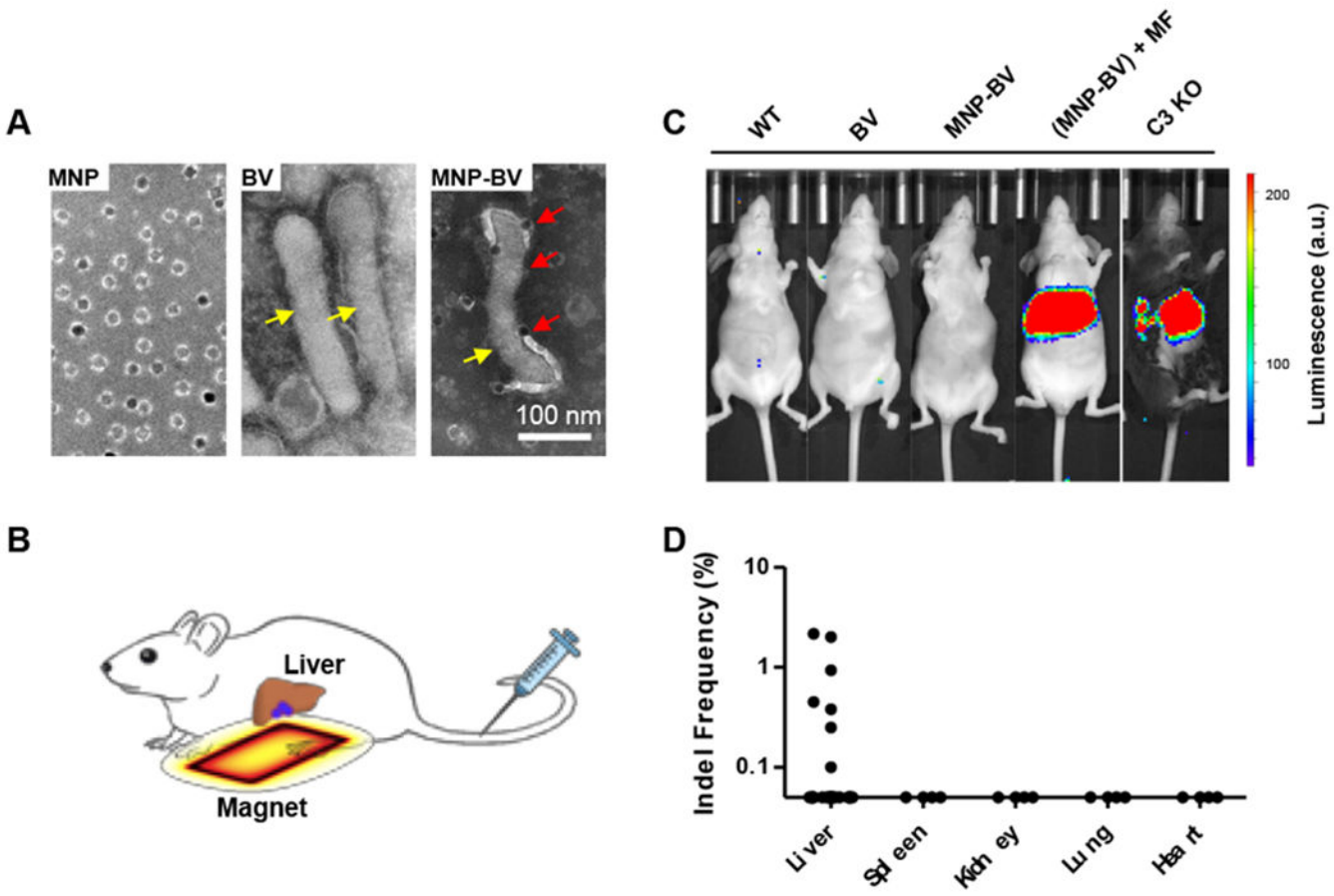

Figure 4. Spatial control of *in vivo* genome editing via nanomagnets.

A. TEM images of MIONs, baculoviral vector (BV) and MION-BV hybrids via TAT peptides. The samples were negatively stained with phosphotungstic acid. **B**. Schematic of MNP-BV mediated transgene delivery in the mouse liver. MNP-BV-LUC was administrated to the mouse through intravenous injection. A block magnet was pressed against the mouse liver to trigger local transgene expression. A contour plot indicated the magnetic force applied to individual MNPs at a distance of 1 mm from the top of the magnet. **C**. Bioluminescence analysis of transgene expression. Nude mice were injected with PBS (wild-type), baculoviral vector (BV) alone, MNP-BV or MNP-BV, followed by magnetic field (MF) treatment for 1 h. In the positive control, C3 knockout mice were injected with BV alone. **D**. Analysis of genome editing in vital organs. (Reproduced with permission from [92], © 2018 Springer Nature.)

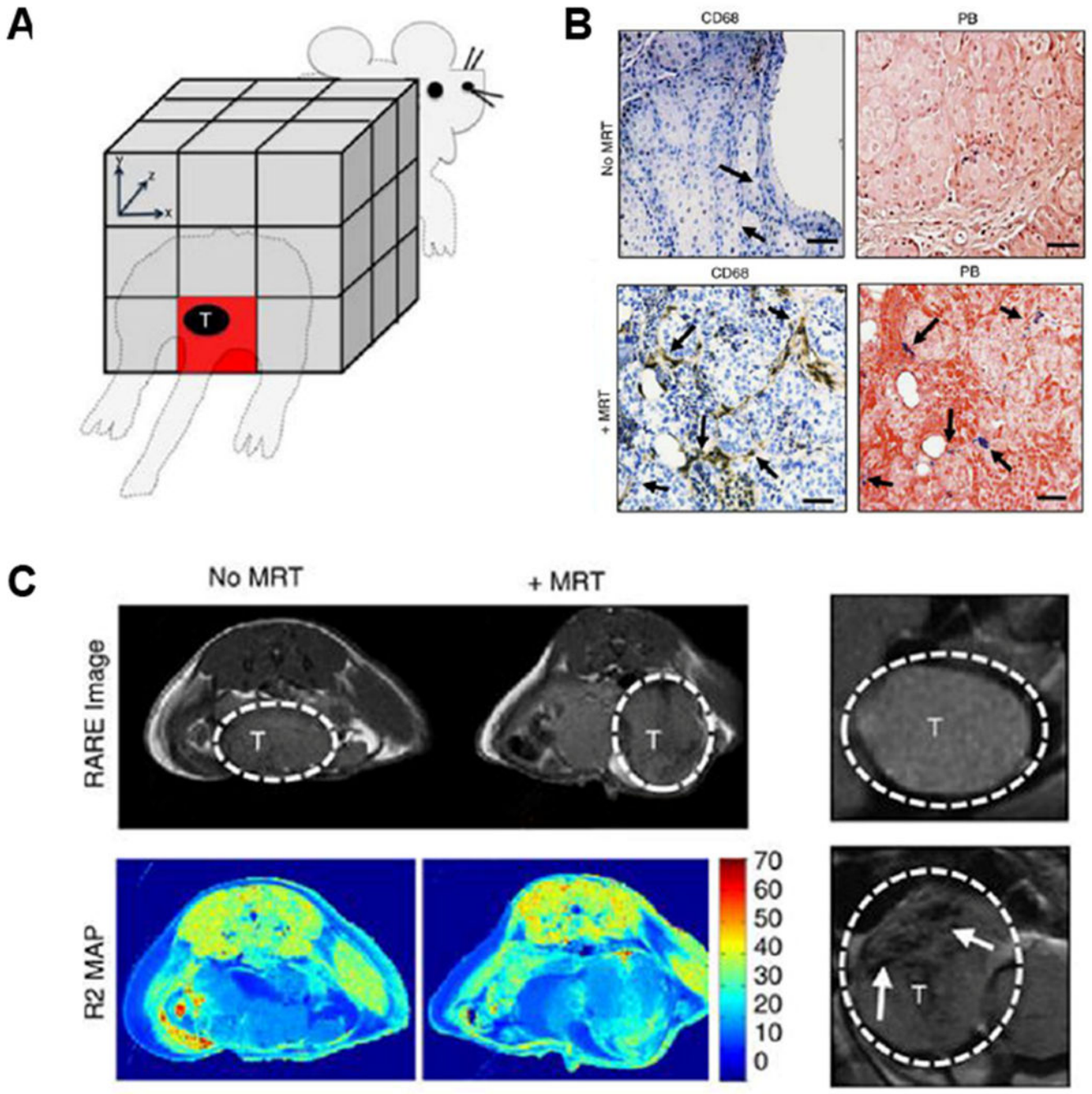

Figure 5. Magnetic resonance targeting of macrophages into primary prostate tumors.

A. Schematic of targeted regions using imaging gradients for magnetic resonance targeting (MRT). **B**. Histological staining of paraffin wax-embedded tumor sections with an anti-human CD68 antibody and Prussian blue (CD68-positive macrophages are brown and SPIO-positive macrophages are blue: see arrows) **C**. Representative RARE images from five mice per group and R2 maps for each group. (Reproduced with permission from [7], © 2015 Macmillan Publishers Limited.)

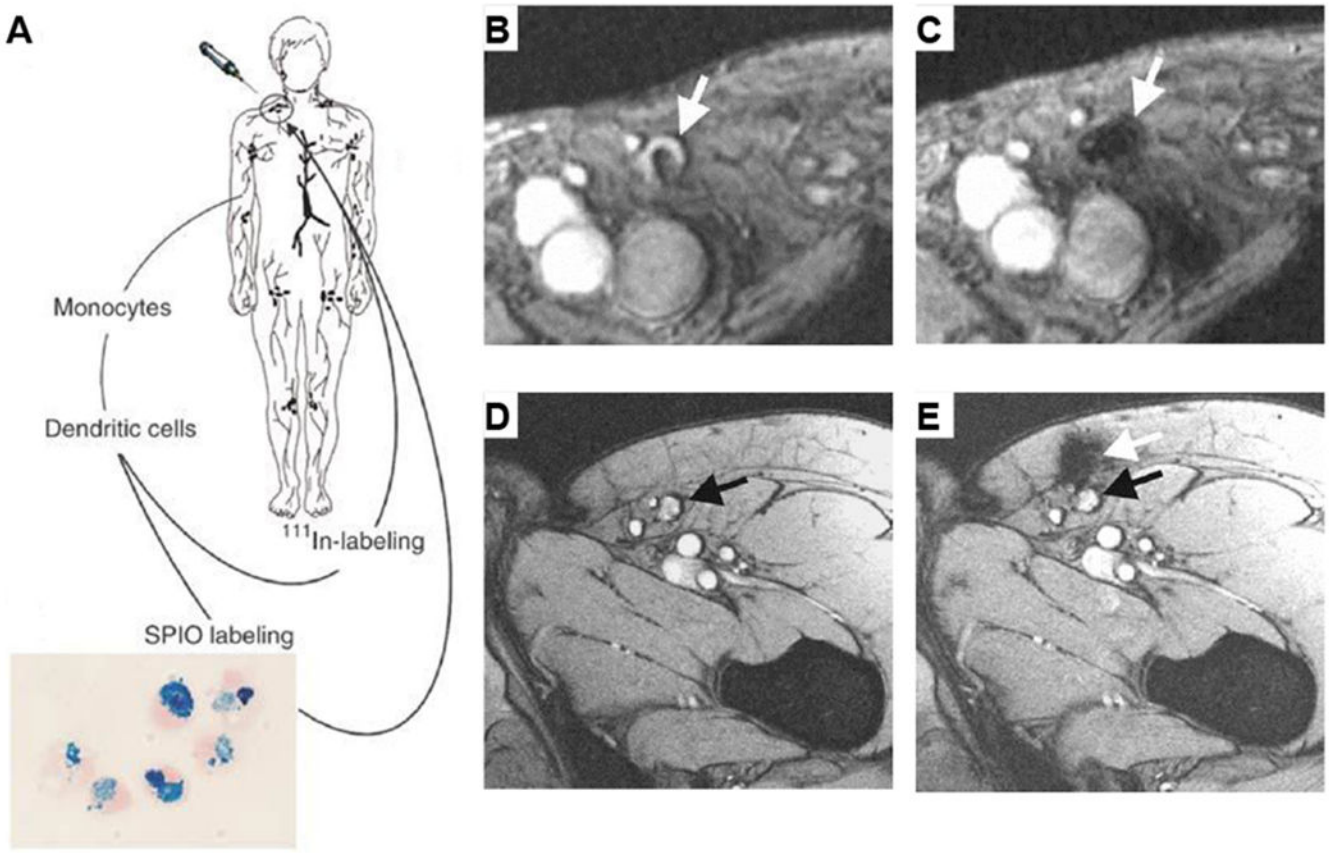

Figure 6. Magnetic resonance tracking of dendritic cells in melanoma patients.

A. Study protocol. Monocytes are obtained by cytopheresis from stage-III melanoma patients, cultured, and labeled with superparamagnetic iron oxide nanoparticles (SPIOs) and ^{111}In. The cells are then injected intranodally into a lymph node basin and their biodistribution is monitored *in vivo* by scintigraphy and MRI at 3 Tesla. **B.** Gradient echo transversal magnetic resonance image before vaccination; and **C**. after vaccination in a patient. There was a decreased signal intensity of the lymph node (white arrow), indicating the accumulation of SPIO-labeled cells. **D.** MRI before vaccination; the inguinal lymph node to be injected is indicated with a black arrow; and **E.** after injection in another patient. The dendritic cells were not accurately delivered into the inguinal lymph node (black arrow) but in the vicinity, in the subcutaneous fat (white arrow). (Reproduced with permission from [116], © 2005 Springer Nature.)

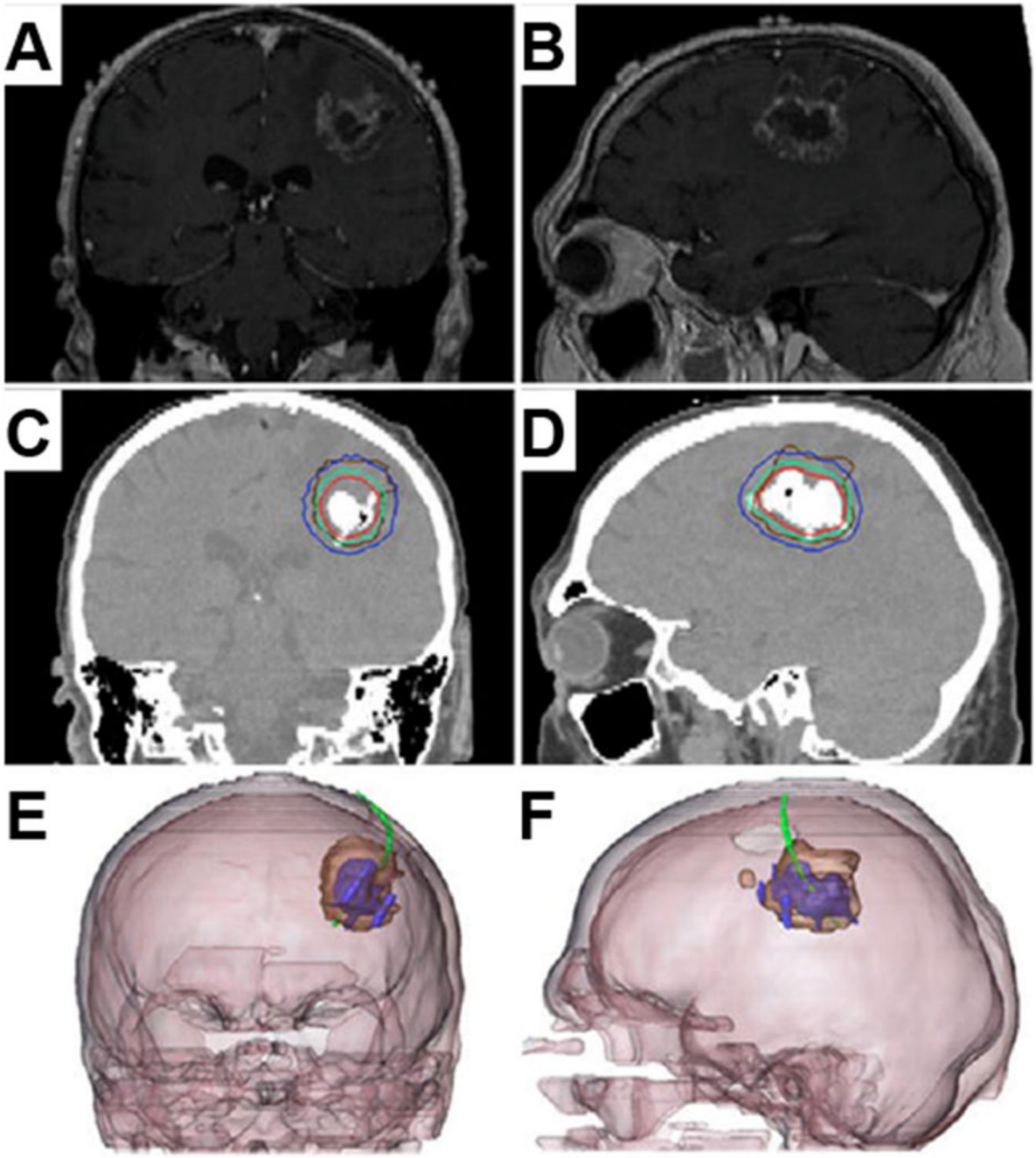

Figure 7. Thermal ablation of brain tumors.

A and **B**. Pre-treatment brain MRI. **C** and **D**. Post-instillation CT showing magnetic nanoparticle deposits as hyperdense areas. Isothermal lines indicate calculated treatment temperatures between 40°C (blue) and 50°C (red). The brown line represents the tumor area. **E** and **F**. 3-D reconstruction of fused MRI and CT showing the tumor (brown), magnetic fluid (blue) and thermometry catheter (green). (Reproduced with permission from [37], © The Author(s) 2010.)

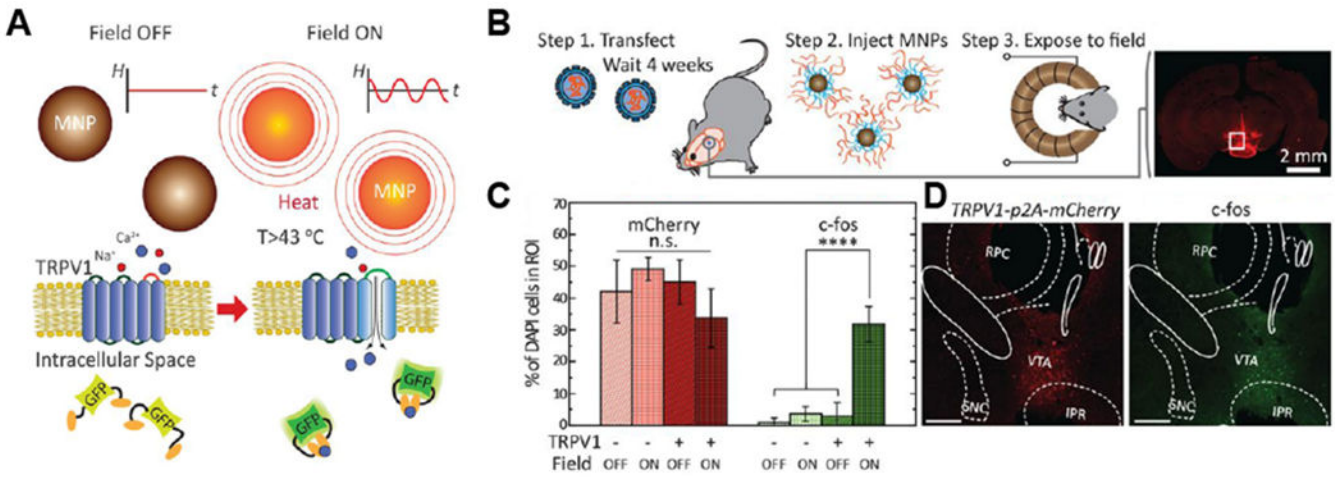

Figure 8. Wireless magnetothermal deep brain stimulation.

A. Wireless ON switch for controlled magnetothermal membrane depolarization of TRPV1^{+} cells. Magnetic field stimulation ("Field ON") triggers calcium ion (Ca^{2+}) influx by opening TRPV1. **B**. Scheme of wireless magnetothermal stimulation *in vivo*. The excitatory neurons in the ventral tegmental area (VTA) was sensitized to heat through the lentiviral delivery of TRPV1, which was followed by magnetic nanoparticles (MNP) injection. Viral transduction was verified by the expression of the reporter gene, mCherry. **C** and **D**. Neuronal excitation was quantified by the extent of activity-dependent expression of the immediate early gene c-fos. Neural activity was only triggered by the magnetic field in the VTA of mice transfected with TRPV1 in the presence of MNPs, resulting in a significantly higher proportion of c-fos $^{+}$ cells. (Reproduced with permission from [158], © 2015 American Association for the Advancement of Science.)

Table 1.

Nanomagnetism and biomedical applications

Mechanism	**Properties of MIONs**	**Magnetic Field**	**Applications**
Magnetic force	The magnetic moment determined by the size and magnetization	A magnetic field with a high gradient	Magnetic drug targeting, magnetofection, magnetic purification of molecules and cells, controllable *in vivo* genome editing, magnetic cell targeting, mechanical cues for cell differentiation, apoptosis, etc.
Magnetic relaxation of protons	Generating a magnetic field for MRI T_1 or T_2 contrast	Uniform magnetic field	Diagnostic imaging, cell tracking, molecular imaging, image-guided drug delivery
Magnetic heating	The magnetic hysteresis determined by magnetic anisotropy, magnetic susceptibility & core size	An alternating magnetic field	Thermal ablation of tumors, magnetic hyperthermia, nanowarming, magnetogenetics, controlled drug release

Table 2

MIONs in Clinical trials and clinical applications

Agents	Formulation	Disease	Status
Ferrofluids [83]	magnetite nanocrystals coated with starch polymers carrying epirubicin (100 nm)	Various cancers	Phase I in 1996
MTC-DOX [84]	Elementary iron coated with activated carbon carrying doxorubicin (0.5-5 μm)	Hepatocellular carcinoma	Phase II/III stopped prematurely in 2005
Endorem® / Feridex I.V.® [103]	Iron oxide nanocrystals coated with dextran (80-150 nm)	Liver tumor detection	FDA approval in 1996; currently discontinued
Resovist®	Iron oxide nanocrystals coated carboxydextran (60 nm)	Liver tumor detection	EMA approval in 2001; currently discontinued
Gastromark® / Lumirem®	Iron oxide nanocrystals coated with silica (300 nm)	GI Tract Imaging	FDA approval in 1996 and EMA approval in 2001; currently discontinued
Sinerem® / Combidex [42]	Iron oxide nanocrystals coated with dextran (20-40 nm)	Detecting occult lymph node metastasis in prostate cancer	Clinical imaging available in the Netherlands
Feraheme® / Ferumoxytol	Iron oxide nanocrystals coated with polyglucose sorbitol carboxymethylethe (30 nm)	Anemia associated with chronic renal failure, iron deficiency anemia	FDA approval in 2009
NanoTherm® [37]	Iron oxide nanocrystals coated aminosilane (15 nm)	Focal thermal ablation treatment of glioblastoma multiforme Focal thermal ablation treatment of intermediate-risk prostate cancer	EMA approval in 2010 Ongoing clinical trials with the Investigational Device Exemption (IDE) approved by FDA